Asociación Argentina
de Mecánica Computacional

Mecánica Computacional Vol XXX, págs. 1591-1614 (artículo completo)
Oscar Möller, Javier W. Signorelli, Mario A. Storti (Eds.)
Rosario, Argentina, 1-4 Noviembre 2011

ENTROPY GENERATION ANALYSIS OF ELECTRO-OSMOTIC FLOW FOR A POWER-LAW FLUID IN A MICROCHANNEL

Juan P. Escandón, Oscar E. Bautista and Eric G. Bautista

Departamento de Termofluidos, SEPI-ESIME Azcapotzalco del IPN, México D. F., 02250, México, jescandon@ipn.mx, http://www.sepi.esimeazc.ipn.mx/

Keywords: entropy generation, power-law model, conjugated heat transfer, electro-osmotic flow, microchannel.

Abstract. In this work the entropy generation in a parallel flat plate microchannel under a purely electro-osmotic flow with a non-Newtonian fluid is analyzed. We considering a fully-developed flow in the velocity profiles; the fluid obeys a constitutive relation based in a power-law model. The temperature fields were obtained by the steady-state analysis of a conjugate heat transfer problem in the fluid and solid walls; the governing energy equation was solved firstly using the numerical successive-over-relaxation method with central finite differences scheme and then an asymptotic solution was introduced to validate the numerical process. Analytical expressions for dimensionless local and global entropy are obtained. The goal of this paper is show the influence of dimensionless parameters involved in the analysis on the temperature profiles, entropy distributions and the Bejan number. The dimensionless parameters are: a flow behavior index, to describe the power-law fluid behavior; an electrokinetic parameter, to indicate the thickness of the Debye length; the Peclet number, as indicator of heat transfer convection; a normalized power generation term, being the ratio of heat flux from the external wall to the Joule heating; a conjugation term, which represents the competition between the longitudinal conductive heat in the microchannel wall to the convective heat transfer in the fluid; a characteristic temperature difference and finally the aspect ratios of the microchannel system, respectively. Additionally is observed the excellent agreement between the numerical and asymptotic solution to the Nusselt number for different conditions in the conjugated heat transfer process.

1 INTRODUCTION

The microfluidic devices are used in the handling of biomedical and chemical analysis. Thus, electrokinetic transport is widely used to control flow and for manipulate sample solutes, include injection, separation, mixing, dilution/concentration, and reaction, (Steffen and Friedhelm, 2007). The electro-osmosis is a mechanism of electrokinetic transport which gives the movement of a volume of an aqueous solution adjacent to a solid charged surface when an external electric field is applied tangentially along the surface (Tang et al., 2007). Due to the rapid development of "Lab-on-a-Chip" technologies during recent years, electro-osmosis is being used extensively as a driving force for manipulating fluid flows for transport and control samples in nano volumes of fluids to biological, chemical and medical diagnostics. Advances in microfluidic devices make possible a complete analysis of fluids in the biochemistry area in a single fabricated chip; therefore, it is fundamental understand the characteristics of fluids flow in microchannels to have an optimum design and precise control of microfluidics devices (Zhao et al., 2008). The physics of electrokinetic phenomena and specifically in the electro-osmotic flow has been extensively reviewed in the literature (Masliyah and Bhattacharjee, 2006; Li, 2004). The heat transfer phenomena of Newtonian fluids in microchannels has been studied by Xuan (2004a, b), and Tang (2004a, b; 2007), they analyze the coupled cases with temperature and conjugates problems in electro-osmotic flow, and the inevitable effect of Joule heating in the flow is emphasized. Although in the literature there are several models proposed to analyze the behavior of non Newtonian fluids, at present, still appear relevant implications on the transport of electrokinetic flows that have not been completely resolved by the scientific community (Das and Chakraborty, 2006). Studies by Zhao et al. (2008), Berli (2008) and Tang et al. (2009), in this regard consider the power-law model for non Newtonian fluids and only solve the hydrodynamics of electro-osmotic flow; Das and Chakraborty (2006) also uses the power-law model to solve analytically the distribution of velocity, temperature and concentration on electro-osmotic flows of non Newtonian biological fluids, but without consider the conjugate heat transfer problem in the microchannel wall. On the other hand there has been a growing interest to optimize thermal systems by entropy generation analysis through certain processes. Entropy generation is always in proportion to thermodynamic irreversibility, both of which are an indispensable part of all real processes. Since there is a strong relationship between entropy generation and lost available work, entropy generation should be reduced for the sake of achieving better performance. During the last two decades, the interest in the entropy generation techniques has experienced a huge growth for the thermal analysis of the flow systems in engineering devices, (Abbassi, 2007). Entropy generation minimization thus came to be utilized as a robust and handy tool for optimization in a wide range of thermal applications (Bejan, 1996). The entropy generation has been studied by Mahmud and Fraser (2006), they consider the power-law for flows of non-Newtonian fluids and heat transfer inside a circular duct, they presents the competition of viscous dissipation and heat transfer irreversibility as a function of flow behavior index. The great deal of researches has been conducted for entropy generation analysis in macro-scale processes and devices; however, in open literature there have been a few numbers of investigations in the field of microfluidic entropy analysis, (Abbassi, 2007). Zhao and Liu (2010), analyze the local entropy generation of electro-osmotic flow due to heat conduction, viscous dissipation and Joule heating in open-end and closed-end micro-channels. Ibáñez and Cuevas (2010), study the entropy generation in a parallel plate microchannel of a magneto-hydrodynamic flow, they solved analytically the conjugate heat transfer problem in the fluid and solid walls, for calculated entropy generation rate. In the present investigation

the conjugate heat transfer problem in a parallel flat plates microchannel will be solved, taking into account a power-law fluid in the flow; then, the local and global entropy generation rate will be calculated, the effect of the main transport parameters involved in the mathematical model on the entropy generation will be presented.

2 METHODOLOGY

2.1 Physical model

The Figure 1 shows a squematic view of the physical model, the fluid flow is through of a microchannel formed by two parallel flat plates of height $2H$ and length L, the wall thickness is H_w; $L/H \gg 1$, $L/H_w \gg 1$. We considered a fluid with a rheological power-law model. The origin of the rectangular coordinates system is placed at the x-symmetry axis of the microchannel and y-axis points out in the transverse direction, which is normal to the surface of the microchannel. The driving forces are provided by an electric field E_x in the axial direction between inlet and outlet of microchannel. For analysis, properties are considered constant with the temperature, the heat transfer in steady state and hydrodynamically developed flow. The fluid enters at a temperature T_0 in $x = 0$. The wall has adiabatic conditions in $x \le 0$ and $x \ge L$. To $0 \le x \le L$, there is a constant heat flux q_0'' in the external wall. The figure shows the high concentration of electric charges in the Debye length, κ^{-1}, inside of the electrical double layer; also, the characteristic velocity u_c in flow direction.

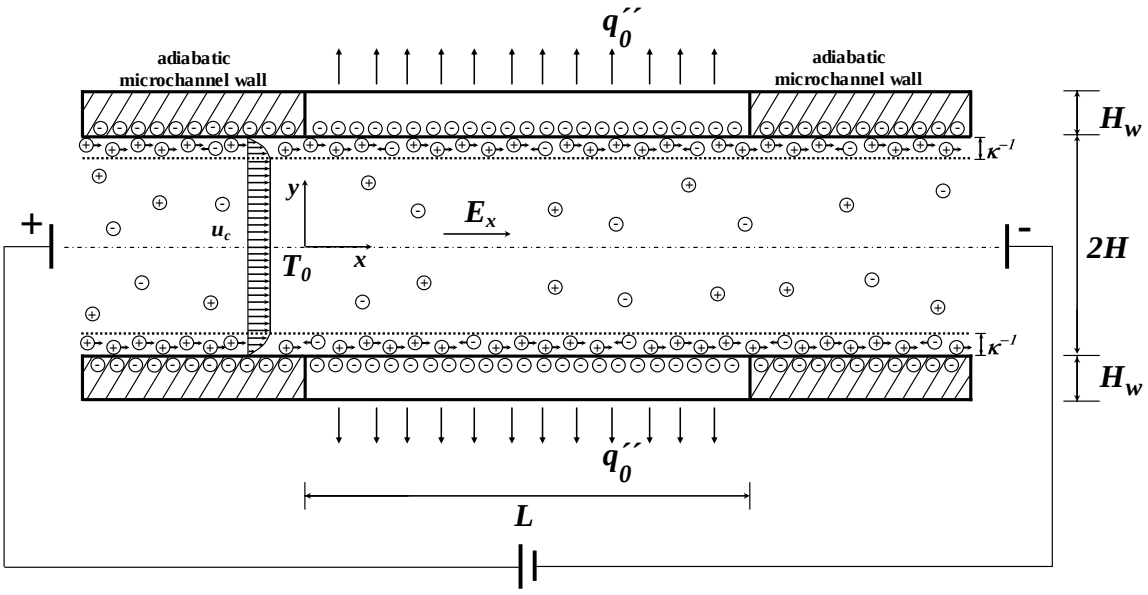

Figure 1: Schematic of electro-osmotic flow between two parallel flat plates.

2.2 Fluid flow and heat transfer modeling

The momentum equation for the assumed conditions is

$$\frac{d}{dy}\tau_{yx} + \rho_e E_x = 0, \tag{1}$$

where τ_{yx} is the shear stress and ρ_e is the net charge density in the diffuse layer within the

electric double layer, respectively defined by (Zhao et al., 2008)

$$\tau_{yx} = m\left(-\frac{du}{dy}\right)^{n-1}\left(\frac{du}{dy}\right), \tag{2}$$

$$\rho_e = -\varepsilon\kappa^2\zeta\frac{\cosh\ \kappa y}{\cosh\ \kappa H}, \tag{3}$$

where $u, \kappa, \varepsilon, \zeta, n$ and m are the axial velocity, the inverse Debye length, the dielectric constant of the fluid, the zeta potential in the shear plane of the electric double layer, the flow behavior index and the flow consistency index, respectively. κ^2 is the Debye-Hückel parameter which is obtained with the assumption of small zeta potentials in the Poisson-Boltzmann equation, (Masliyah and Bhattacharjee, 2006). So the Eq. (1) is transformed in

$$-\frac{d}{dy}\left[m\left(-\frac{du}{dy}\right)^n\right] = \varepsilon\kappa^2\zeta E_x\frac{\cosh\ \kappa y}{\cosh\ \kappa H}, \tag{4}$$

with the corresponding boundary conditions

$$u\ \ x, y = H\ \ = 0, \tag{5}$$

$$\left.\frac{du}{dy}\right|_{x,y=0} = 0. \tag{6}$$

After integrate once the Eq. (4) and using the Eq. (6), the velocity gradient is given as

$$\frac{du}{dy} = -\left[-\frac{\varepsilon\kappa\zeta E_x}{m}\frac{\sinh\ \kappa y}{\cosh\ \kappa H}\right]^{1/n}. \tag{7}$$

The energy equation for the fluid is given by

$$\rho C_{pf} u\frac{\partial T_f}{\partial x} = k_f\frac{\partial^2 T_f}{\partial x^2} + k_f\frac{\partial^2 T_f}{\partial y^2} + \tau_{yx}\left(\frac{du}{dy}\right) + \sigma E_x^2, \tag{8}$$

where ρ, C_{pf}, T_f, k_f and σ are the density, the specific heat, the temperature, the thermal conductivity and the electrical conductivity, respectively; x, y are the axial and the transversal coordinate. The boundary conditions associated with Eq. (8) are

$$T_f\ \ x = 0, y\ \ = T_0, \tag{9}$$

$$\left.\frac{\partial T_f}{\partial x}\right|_{x=L,y} = 0, \tag{10}$$

$$\left.\frac{\partial T_f}{\partial y}\right|_{x,y=0} = 0, \tag{11}$$

$$T_w\ x,y=H\ =T\ x,y=H\ ;-k_w\frac{\partial T_w}{\partial y}\bigg|_{x,y=H}=-k_f\frac{\partial T_f}{\partial y}\bigg|_{x,y=H}, \tag{12}$$

where T_w, and k_w are the temperature and the thermal conductivity in the wall, respectively. The energy equation for the solid is given by

$$\frac{\partial^2 T_w}{\partial x^2}+\frac{\partial^2 T_w}{\partial y^2}=0, \tag{13}$$

with their boundary conditions associated

$$\frac{\partial T_w}{\partial x}\bigg|_{x=0,L;y}=0, \tag{14}$$

$$-k_w\frac{\partial T_w}{\partial y}\bigg|_{y=H+H_W}=q_0''. \tag{15}$$

2.3 Second law analysis

Taking account for laminar regimen in electro-osmotic flow, the local volumetric entropy generation due to heat conduction, viscous dissipation and Joule heating in the fluid region of microchannel can be represented respectively as (Zhao and Liu, 2010)

$$S'''_{G_{cond-fluid}}=\frac{k_f}{T_f^2}\left[\left(\frac{\partial T_f}{\partial x}\right)^2+\left(\frac{\partial T_f}{\partial y}\right)^2\right], \tag{16}$$

$$S'''_{G_{f-fluid}}=\frac{1}{T_f}\left[\tau_{yx}\left(\frac{du}{dy}\right)\right], \tag{17}$$

$$S'''_{G_{j-fluid}}=\frac{\sigma E_x^2}{T_f}, \tag{18}$$

in the case of the solid region of microchannel, the local volumetric entropy generation due to heat conduction can be described by (Abbassi, 2007)

$$S'''_{G_{cond-solid}}=\frac{k_w}{T_w^2}\left[\left(\frac{\partial T_w}{\partial x}\right)^2+\left(\frac{\partial T_w}{\partial y}\right)^2\right], \tag{19}$$

2.4 Dimensionless mathematical model for heat transfer process

Defining the following dimensionless variables

$$X=\frac{x}{L}, \tag{20}$$

$$Y=\frac{y}{H}, \tag{21}$$

$$U=\frac{u}{u_c}, \tag{22}$$

$$\bar{T}_f = \frac{T_f - T_0}{\Delta T_c}, \tag{23}$$

$$\bar{T}_w = \frac{T_w - T_0}{\Delta T_c}, \tag{24}$$

$$Z = \frac{y - H}{H_w}, \tag{25}$$

where X and Y are the dimensionless axial and the transversal coordinates respectively; U , $\bar{T}_f$, $\bar{T}_w$ and Z are the velocity, the temperature in the fluid, the temperature in the solid and the transversal coordinate to analyze the solid wall, dimensionless, respectively. $u_c = n\kappa^{1-n/n} - \varepsilon\zeta E_x/m^{1/n}$ is the generalized Smoluchowski velocity for power-law fluids (Zhao et al., 2008). The characteristic temperature change was chosen as $\Delta T_c = \sigma E_x^2 H^2 / k_f$. By introducing the dimensionless variables from Eqs. (20-23) in Eqs. (8-12) the dimensionless energy equation in the fluid region in the microchannel is obtained

$$\beta PeU \frac{\partial \bar{T}_f}{\partial X} = \beta^2 \frac{\partial^2 \bar{T}_f}{\partial X^2} + \frac{\partial^2 \bar{T}_f}{\partial Y^2} + \Pr Ec\left(-\frac{dU}{dY}\right)^{n+1} + 1, \tag{26}$$

and their boundary conditions

$$\bar{T}_f \;\; X = 0, Y \;\; = 0, \tag{27}$$

$$\left.\frac{\partial \bar{T}_f}{\partial X}\right|_{X=1,Y} = 0, \tag{28}$$

$$\left.\frac{\partial \bar{T}_f}{\partial Y}\right|_{X,Y=0} = 0, \tag{29}$$

$$\bar{T}_f \;\; X, Y = 1 \; = \bar{T}_w \;\; X, Z = 0 \;, \tag{30}$$

in addition to Eq. (30) was considered the next boundary condition in the internal interface of microchannel from the Eq. (12)

$$\left.\frac{\bar{\alpha}}{\bar{\varepsilon}^2}\frac{\partial \bar{T}_w}{\partial Z}\right|_{X,Z=0} = \left.\frac{\partial \bar{T}_f}{\partial Y}\right|_{X,Y=1} . \tag{31}$$

Then, the energy equation in the fluid and their boundary conditions leaves the following dimensionless parameters

$$\beta = \frac{H}{L}, \tag{32}$$

$$\bar{\varepsilon} = \frac{H_w}{L}, \tag{33}$$

$$Pe = \frac{\rho C_{pf} u_c H}{k_f}, \tag{34}$$

$$\bar{\alpha} = \frac{k_w}{k_f}\frac{H}{L}\frac{H_w}{L}, \tag{35}$$

$$\mathrm{Pr} = \frac{mC_{pf}}{k_f}, \tag{36}$$

$$Ec = \frac{u_c^{n+1}}{C_{pf}\Delta T_c H^{n-1}}, \tag{37}$$

where β and $\bar{\varepsilon}$ are the aspect ratios in the fluid and solid region, respectively; Pe and $\bar{\alpha}$ are the Peclet number and the conjugation term which determines the basic heat transfer regimes between fluid and solid sections in the microchannel; Pr is the Prandtl number and Ec is the modified Eckert number, (Mahmud and Fraser, 2006). By using the Eqs. (21) and (22) into Eq. (7) we have the dimensionless velocity

$$\frac{dU}{dY} = -\left[\left(\frac{\bar{\kappa}}{n}\right)^n \frac{\sinh\ \bar{\kappa}Y}{\cosh\ \bar{\kappa}}\right]^{1/n}, \tag{38}$$

Zhao et al. (2008), gives an approximate analytical solution to the above relationship. $\bar{\kappa} = \kappa H$ is the electrokinetic parameter, (Masliyah and Bhattacharjee, 2006). The Eq. (38) takes in consideration the next boundary condition, from Eq. (5)

$$U\ \ X, Y = 1\ \ = 0. \tag{39}$$

The dimensionless energy equation for the microchannel wall is obtained by introducing the dimensionless variables given in the Eqs. (20), (24-25) in the Eqs. (13-15), then we have

$$\bar{\alpha}\frac{\partial^2 \bar{T}_w}{\partial X^2} + \frac{\bar{\alpha}}{\bar{\varepsilon}^2}\frac{\partial^2 \bar{T}_w}{\partial Z^2} = 0, \tag{40}$$

and their boundary conditions

$$\left.\frac{\partial \bar{T}_w}{\partial X}\right|_{X=0,1;Z} = 0, \tag{41}$$

$$\left.\frac{\partial \bar{T}_w}{\partial Z}\right|_{X,Z=1} = -\frac{\bar{\varepsilon}^2}{\bar{\alpha}}\Lambda, \tag{42}$$

where

$$\Lambda = \frac{q_0''}{\sigma E_x^2 H}, \tag{43}$$

Λ, is the normalized power generation term being the ratio of heat flux from the external wall to the Joule heating. For the solid region in the microchannel, is necessary considered the boundary condition in the internal interface given by Eqs. (30-31).

2.5 Order of magnitude analysis

The order of magnitude of the shear stress can be obtained from Zhao et al. (2008) as

$$\tau_{yx} \sim \varepsilon\kappa\zeta E_x, \tag{44}$$

and the order of magnitude of the velocity gradient or strain rate is

$$\frac{du}{dy} \sim \frac{u_c}{H}. \tag{45}$$

So, considering typical values in electro-osmotic flows and by comparing the order of magnitude of the viscous dissipation and the power generation terms in Eq. (8), the following relationship is obtained

$$\frac{\sigma E_x^2}{\varepsilon\kappa\zeta E_x\left(\frac{u_c}{H}\right)} \gg 1, \tag{46}$$

this order of magnitude indicates that the viscous dissipation effect can be neglected in the energy equation for the fluid region. Now, to obtained the scales of the temperature changes in the fluid region, we compare the diffusive terms with the power generation term in Eq. (8), as follows

$$\Delta T_{f,x} \sim \frac{\sigma E_x^2 L^2}{k_f}, \tag{47}$$

$$\Delta T_{f,y} \sim \frac{\sigma E_x^2 H^2}{k_f}, \tag{48}$$

where, $\Delta T_{f,x}$ and $\Delta T_{f,y}$ are the temperature changes in the directions x and y, respectively. Then, by comparing the Eq. (47) and (48) we have

$$\frac{\Delta T_{f,x}}{\Delta T_{f,y}} \sim \left(\frac{L}{H}\right)^2 \gg 1, \tag{49}$$

this result shows that the most important temperature changes are in the longitudinal direction. In addition, due to adiabatic boundary conditions in the microchannel walls, an order of magnitude of energy balance at the microchannel wall indicates, in a first approximation, that the most of the heat generated by Joule heating effect is of the order of magnitude of transverse conductive heat into the microchannel wall and also of the same order of the magnitude of the heat losses, that is

$$\sigma E_x^2 H \sim k_f \frac{\Delta T_{f,y}}{H} \sim k_w \frac{\Delta T_{w,y}}{H_w} \sim q_0'', \tag{50}$$

where $\Delta T_{w,y}$ is the temperature change in y direction in the microchannel wall. By considering the total temperature change in the transversal coordinate ΔT_y of microchannel system is then of order

$$\Delta T_y \sim \Delta T_{f,y} + \Delta T_{w,y}. \tag{51}$$

Combining the Eqs. (50) and (51), can be shown that

$$\frac{\Delta T_{f,y}}{\Delta T_y} \sim \frac{1}{1+\frac{\bar{\varepsilon}^2}{\bar{\alpha}}}, \tag{52}$$

$$\frac{\Delta T_{w,y}}{\Delta T_y} \sim \frac{\frac{\bar{\varepsilon}^2}{\bar{\alpha}}}{1+\frac{\bar{\varepsilon}^2}{\bar{\alpha}}}, \tag{53}$$

therefore, the total temperature change must be then of the order

$$\Delta T_y \sim \Delta T_{f,y}\left[1+\frac{\bar{\varepsilon}^2}{\bar{\alpha}}\right]. \tag{54}$$

From Eq. (52) and (53) we can obtain interesting asymptotic relevant limits, which dictate the different physical regimes of the conjugate heat transfer process. Basically, for electro-osmotic flows, typical limits for the dimensionless parameters are $\bar{\alpha}/\bar{\varepsilon}^2 \ll 1, \bar{\alpha}/\bar{\varepsilon}^2 \sim 1, \bar{\alpha}/\bar{\varepsilon}^2 \gg 1$ all with $\bar{\alpha} \ll 1$. For values of $\bar{\alpha}/\bar{\varepsilon}^2 \ll 1$, from Eqs. (52) and (53) we obtain

$$\frac{\Delta T_{f,y}}{\Delta T_y} \sim \frac{\bar{\alpha}}{\bar{\varepsilon}^2}; \frac{\Delta T_{w,y}}{\Delta T_y} \sim 1, \tag{55}$$

from Eq. (55), the transverse temperature drop in the fluid is small of order of $\bar{\alpha}/\bar{\varepsilon}^2$ at most, and the transverse temperature variations in the microchannel wall is of order of the total temperature drop. For values of $\bar{\alpha}/\bar{\varepsilon}^2 \sim 1$, we obtain from the same order relationships

$$\frac{\Delta T_{f,y}}{\Delta T_y} \sim \frac{1}{2}; \frac{\Delta T_{w,y}}{\Delta T_y} \sim \frac{1}{2}, \tag{56}$$

in the above equation, the transverse temperature variations in the wall as well as in the fluid, compared with the total temperature drop, are of the same order. Finally, for values of $\bar{\alpha}/\bar{\varepsilon}^2 \gg 1$, we obtain

$$\frac{\Delta T_{f,y}}{\Delta T_y} \sim 1; \frac{\Delta T_{w,y}}{\Delta T_y} \sim \frac{\bar{\varepsilon}^2}{\bar{\alpha}}, \tag{57}$$

for the Eq. (57) the transverse temperature drop in the fluid is of the same order that the total temperature drop and the transverse temperature variations in the microchannel wall compared with total temperature drop ΔT_y are very small, of order $\bar{\varepsilon}^2/\bar{\alpha}$ at most.

2.6 Asymptotic solution for the temperature fields

In this section, we propose the next regular expansions series, in powers of $\bar{\alpha}$, for the dimensionless temperatures of the fluid and microchannel wall, respectively

$$\bar{T}_f \sim \bar{T}_{f0}\ X\ + \bar{\alpha}\bar{T}_{f1}\ X,Y\ + ..., \tag{58}$$

and

$$\bar{T}_w \sim \bar{T}_{w0}\ X,Z\ + \bar{\alpha}\bar{T}_{w1}\ X,Z\ + \ldots, \tag{59}$$

where we have assumed that the temperature in the fluid is function of X in a first approximation, by the reason mentioned in Eq. (49), and the temperature in the wall depends on X and Z. The Eqs. (58) and (59) are introduced in the energy equations, first to the microchannel wall

$$\frac{\partial^2 \bar{T}_{w0}}{\partial Z^2} + \bar{\alpha}\frac{\partial^2 \bar{T}_{w1}}{\partial Z^2} + \ldots = 0, \tag{60}$$

with the following boundary conditions

$$X,Z=1 : \frac{\partial \bar{T}_{w0}}{\partial Z} + \bar{\alpha}\frac{\partial \bar{T}_{w1}}{\partial Z} + \ldots = -\frac{\bar{\varepsilon}^2}{\bar{\alpha}}\Lambda, \tag{61}$$

$$\bar{T}_{w0} + \bar{\alpha}\bar{T}_{w1} + \ldots \ _{X,Z=0} = \bar{T}_{f0} + \bar{\alpha}\bar{T}_{f1} + \ldots \ _{X,Y=1}, \tag{62}$$

and for the fluid

$$\beta PeU\left[\frac{\partial \bar{T}_{f0}}{\partial X} + \bar{\alpha}\frac{\partial \bar{T}_{f1}}{\partial X} + \ldots\right] = \beta^2\left[\frac{\partial^2 \bar{T}_{f0}}{\partial X^2} + \bar{\alpha}\frac{\partial^2 \bar{T}_{f1}}{\partial X^2} + \ldots\right] + \bar{\alpha}\frac{\partial^2 \bar{T}_{f1}}{\partial Y^2} + 1, \tag{63}$$

the Eq. (63) has to be solved with the boundary conditions

$$X=0,Y\ : \bar{T}_{f0} + \bar{\alpha}\bar{T}_{f1} + \ldots = 0, \tag{64}$$

$$X=1,Y\ : \frac{\partial \bar{T}_{f0}}{\partial X} + \bar{\alpha}\frac{\partial \bar{T}_{f1}}{\partial X} + \ldots = 0, \tag{65}$$

$$X,Y=0\ : \frac{\partial \bar{T}_{f0}}{\partial Y} + \bar{\alpha}\frac{\partial \bar{T}_{f1}}{\partial Y} + \ldots = 0. \tag{66}$$

In addition to the boundary conditions given by Eqs. (62) and (64-66), we need the compatibility condition at the internal surface of the microchannel wall given by the continuity heat flux; in terms of the expansions (58) and (59), we have that

$$\frac{\bar{\alpha}}{\bar{\varepsilon}^2}\left[\frac{\partial \bar{T}_{w0}}{\partial Z} + \bar{\alpha}\frac{\partial \bar{T}_{w1}}{\partial Z} + \ldots\right]_{X,Z=0} = \left[\frac{\partial \bar{T}_{f0}}{\partial Y} + \bar{\alpha}\frac{\partial \bar{T}_{f1}}{\partial Y} + \ldots\right]_{X,Y=1}. \tag{67}$$

As consequence of Eq. (49) we can integrate the energy equation for the fluid, Eq. (63), in the transverse direction and apply the appropriate boundary conditions from Eqs. (61-62) and (64-67). After collecting terms of the same power of $\bar{\alpha}$, we obtain up to zeroth-order terms, the following equation

$$O\ \bar{\alpha}^0\ : \beta Pe\frac{\partial \bar{T}_{f0}}{\partial X}k_1 = \beta^2\frac{\partial^2 \bar{T}_{f0}}{\partial X^2} - \Lambda + 1, \tag{68}$$

where $k_1 = \int_{Y=0}^{Y=1} U\ \eta; n, \bar{\kappa},\ dY.$

The general solution for the Eq. (68), after applying the boundary conditions, is given by

$$\bar{T}_{f0}\ X\ = \frac{\Lambda - 1\left[\exp\left(\frac{k_1 Pe}{\beta}\ X - 1\right) - \exp\left(-\frac{k_1 Pe}{\beta}\right)\right]}{k_1 Pe^{\ 2}} + \frac{1-\Lambda\ X}{k_1 \beta Pe}. \tag{69}$$

Similarly, up to terms of order $\bar{\alpha}^0$, the solution for the energy equation in the solid wall, Eq. (60), after applying the corresponding boundary conditions, is written as

$$\bar{T}_{w0}\ X, Z\ = -\frac{\bar{\varepsilon}^2}{\bar{\alpha}}\Lambda Z + \bar{T}_{f0}\ X\ . \tag{70}$$

On the other hand, the reduced Nusselt number for this problem can be written as

$$\mathrm{Nu} = -\frac{H\left.\frac{\partial T_f}{\partial y}\right|_{x,y=H}}{T_f\ x, y = H\ - T_{w-av}}, \tag{71}$$

where T_{w-av} is the average value of the microchannel wall temperature at a given section. In terms of dimensionless variables, Eq. (71) transforms to

$$\mathrm{Nu} = \frac{-\left.\frac{\partial \bar{T}_{f0}}{\partial Y}\right|_{X,Y=1}}{\bar{T}_{f0} - \bar{T}_{w0-av}}, \tag{72}$$

in Eq. (72), $\bar{T}_{w0-av}$ is the dimensionless mean microchannel wall temperature defined by

$$\bar{T}_{w0-av} = \frac{\int_0^1 \bar{T}_{w0}\ X, Z\ dZ}{\int_0^1 dZ}, \tag{73}$$

and $\left.\partial \bar{T}_{f0}/\partial Y\right|_{X,Y=1}$ is given by Eq. (67). Substituting the corresponding variables into Eq. (72), we obtain

$$\mathrm{Nu} = \frac{2\bar{\alpha}}{\bar{\varepsilon}^2}. \tag{74}$$

2.7 Dimensionless second law analysis

2.7.1 Local entropy generation

By introducing the next dimensionless variable, (Ibáñez and Cuevas, 2010) in the second law analysis

$$N_s = \frac{S_G'''}{k_f / H^2}, \tag{75}$$

we have in dimensionless terms, the local entropy generation rate also called dimensionless entropy generation number, for heat conduction, viscous dissipation and Joule heating in the fluid region, from Eqs. (16-18) and using the appropriate dimensionless variables from Eqs. (20-25), we have respectively

$$N_{S_{cond-fluid}} = \frac{\Omega^2}{\Omega\bar{T}_f + 1^{\,2}}\left[\beta^2\left(\frac{\partial\bar{T}_f}{\partial X}\right)^2 + \left(\frac{\partial\bar{T}_f}{\partial Y}\right)^2\right], \tag{76}$$

$$N_{S_{f-fluid}} = \Pr Ec\frac{\Omega}{\Omega\bar{T}_f + 1}\left(-\frac{dU}{\partial Y}\right)^{n+1}, \tag{77}$$

$$N_{S_{j-fluid}} = \frac{\Omega}{\Omega\bar{T}_f + 1}, \tag{78}$$

$$N_{S_{fluid}} = N_{S_{cond-fluid}} + N_{S_{f-fluid}} + N_{S_{j-fluid}}, \tag{79}$$

and for heat conduction in the solid region, from Eq. (19)

$$N_{S_{solid}} = N_{S_{cond-solid}} = \frac{\bar{\alpha}}{\bar{\varepsilon}^2}\frac{\beta}{\bar{\varepsilon}}\frac{\Omega}{\Omega\bar{T}_w + 1^{\,2}}\left[\bar{\varepsilon}^2\left(\frac{\partial\bar{T}_w}{\partial X}\right)^2 + \left(\frac{\partial\bar{T}_w}{\partial Z}\right)^2\right], \tag{80}$$

where $\Omega = \Delta T_c / T_0$ is the dimensionless temperature difference, (Mahmud and Fraser, 2006). Now, by appropriated substitution of the Eqs. (38), (69) and (70) in Eqs. (76-77) and (80), we have the next expressions in first approximation to the entropy generation

$$N_{S_{cond-fluid}} = \left\{\frac{\Lambda - 1}{k_1 Pe}\frac{\Omega}{\Omega\bar{T}_{f0} + 1}\left[\exp\left\{\frac{k_1 Pe}{\beta}\ X - 1\right\} - 1\right]\right\}, \tag{81}$$

$$N_{S_{f-fluid}} = \Pr Ec\frac{\Omega}{\Omega\bar{T}_f + 1}\left\{\left(\frac{\bar{\kappa}}{n}\right)^n \frac{\sinh\ \bar{\kappa}Y}{\cosh\ \bar{\kappa}}\right\}^{n+1/n}, \tag{82}$$

$$N_{S_{cond-solid}} = \frac{\bar{\alpha}}{\bar{\varepsilon}^2}\frac{\beta\bar{\varepsilon}\Omega^2}{\Omega\bar{T}_w + 1^{\,2}}\left[\left(\frac{\Lambda - 1}{k_1 Pe\beta}\right)^2\left\{\exp\left\{\frac{k_1 Pe}{\beta}\ X - 1\right\} - 1\right\}^2 + \left(-\frac{\bar{\varepsilon}}{\bar{\alpha}}\Lambda\right)^2\right]. \tag{83}$$

2.7.2 Fluid friction and heat transfer irreversibility

The entropy is generated in a process or system due to presence of irreversibility; in a convection problem both fluid friction and heat transfer contribute to the rate of entropy generation. To analyze the relative dominance of entropy generation contributions, Bejan (1996), introduce irreversibility distribution ratio ϕ which is defined by the ratio of entropy generation due fluid friction to heat transfer. For this work and for typical values in electro-osmotic flows ϕ can be written as, (Abbassi, 2007)

$$\phi = \frac{N_{S_{f-fluid}}}{N_{S_{cond-fluid}} + N_{S_{j-fluid}} + N_{S_{cond-solid}}} \ll 1. \tag{84}$$

Paolleti et al. (1989), proposes the irreversibility distribution ratio in different way and introduce the Bejan number *Be*, defined and evaluated for this work as

$$Be = \frac{1}{1+\phi} \approx 1, \tag{85}$$

then for this work, the entropy generation is dominated by heat transfer process in the microchannel system.

2.7.3 Global entropy generation

In order to facilitate the comparison between the results and for better insight to the effect of dimensionless parameters under investigation, the volumetric averaged or global entropy generation rate can be evaluated using the following expression

$$\bar{N}_S = \frac{1}{\forall} \int_{\forall} N_S d\forall, \tag{86}$$

where $\forall$ represent the volume of the microchannel. The Eq. (86) is transformed to the fluid and solid region as

$$\bar{N}_S = \frac{1}{\forall_f} \int_{\forall_f} N_{S\,fluid} d\forall_f + \frac{1}{\forall_s} \int_{\forall_s} N_{S\,solid} d\forall_s. \tag{87}$$

From the Eq. (87) and with help the Eqs. (78) and (81-83) we obtain

$$\bar{N}_{S_{fluid}} = \frac{1}{\forall_f} \int_{\forall_f} N_{S\,fluid} d\forall_f = \int_0^1 \int_0^1 N_{S_{cond-fluid}} + N_{S_{f-fluid}} + N_{S_{j-fluid}} \; dXdY, \tag{88}$$

$$\bar{N}_{S_{solid}} = \frac{1}{\forall_s} \int_{\forall_s} N_{S\,solid} d\forall_s = \int_0^1 \int_0^1 N_{S_{cond-solid}} dXdZ, \tag{89}$$

taking each term from the above equations, the volumetric average entropy for the fluid region is

$$\int_0^1 \int_0^1 N_{S_{cond-fluid}} dXdY = \int_0^1 \left\{ \frac{\Lambda - 1}{k_1 Pe} \frac{\Omega}{\Omega \bar{T}_{f0} \; X \; + 1} \left[\exp\left\{ \frac{k_1 Pe}{\beta} \; X - 1 \right\} - 1 \right] \right\}^2 dX, \tag{90}$$

$$\int_0^1 \int_0^1 N_{S_{f-fluid}} dXdY = \int_0^1 \Pr Ec \left\{ \left(\frac{\bar{\kappa}}{n} \right)^n \frac{\sinh \; \bar{\kappa} Y}{\cosh \; \bar{\kappa}} \right\}^{n+1/n} \int_0^1 \frac{\Omega}{\Omega \bar{T}_f \; X \; + 1} dXdY, \tag{91}$$

$$\int_0^1 \int_0^1 N_{S_{j-fluid}} dXdY = \int_0^1 \frac{\Omega}{\Omega \bar{T}_f \; X \; + 1} dX, \tag{92}$$

and finally for the solid region

$$\int_0^1 \int_0^1 N_{S_{cond-solid}} dXdY = \int_0^1 -\left(\frac{\bar{\alpha}}{\bar{\varepsilon}^2} \right)^2 \frac{\beta \bar{\varepsilon}}{\Lambda} \left[\frac{\left(\frac{\Lambda - 1}{k_1 Pe \beta} \right)^2 \left\{ \exp\left\{ \frac{k_1 Pe}{\beta} \; X - 1 \right\} - 1 \right\}^2 + \left(-\frac{\bar{\varepsilon}}{\bar{\alpha}} \Lambda \right)^2}{\left(\bar{T}_{f0} \; X \; + \frac{1}{\Omega} \right) \left\{ 1 - \frac{\bar{\alpha}}{\bar{\varepsilon}^2} \frac{1}{\Lambda} \left(\bar{T}_{f0} \; X \; + \frac{1}{\Omega} \right) \right\}} \right] dX, \tag{93}$$

2.8 Numerical Solution

The mathematical model was solved by a conventional numerical scheme with central finite differences. The energy equations for the fluid and solid wall were solved by an iterative process. Firstly, we solved the temperature in the solid wall with the corresponding boundary conditions, guessing an arbitrary specified temperature at the internal surface in order to initialize the process. Consequently, a temperature field is obtained in the microchannel wall, from which a temperature gradient at the internal solid-liquid interface is obtained. This temperature gradient can be used as a boundary condition into Eq. (31), in order to solve the energy equation in the fluid. In this manner, a temperature field in the fluid is obtained. Once that the solid and fluid regions are solved, we compare the interfacial temperature $\bar{T}_f\ X,Y=1$ and $\bar{T}_w\ X,Z=0$, such that the condition $\left|\bar{T}_f\ X,Y=1-\bar{T}_w\ X,Z=0\right|\leq 10^{-5}$ is fulfilled. The equations in the section 2.4 were solved numerically for different values of the involved dimensionless parameters n, Pe, Λ, $\bar{\kappa}$, $\bar{\varepsilon}$ and $\bar{\alpha}$. For numerical calculations, in the fluid, we obtain good results using a grid size of $\Delta X=0.005$, $\Delta Y=0.005$, with $M=200$ nodes in the transversal direction Y and $N=200$ nodes in the longitudinal direction X for the fluid. Similarly, in the solid microchannel wall, we use a grid size $M=200$ nodes in the transversal direction Z and $N=200$ nodes in the longitudinal direction X . The resulting system of linear equations is represented by a matrix of order NxM for each region, which was solved by using the iterative method Successive-Over-Relaxation (Hoffman, 2001), with a tolerance of 10^{-8}. The velocity profiles in the Eq. (38) were solved by Zhao et al, (2008) and introduced for the solution in this work. In order to obtain the numerical results for the Nusselt number, the Eq. (72) also was discretized. To solve the local entropy generation, we used of approximated results to the temperature profiles from Eqs. (69) and (70); finally the global energy generation was obtained with a conventional numeric integration.

3 RESULTS AND DISCUSSIONS

For the numerical and analytical calculations in this work, typical transport properties and geometrical parameters listed in Table 1 were used (Steffen and Friedhelm, 2007; Das and Chakraborty, 2006; Masliyah and Bhattacharjee, 2006; Zhao et al., 2008; Tang et al., 2009, 2004b, 2007).

Parameter	Value	Unit	Parameter	Value	Unit
H	$\sim 10^{-5}$-10^{-4}	(m)	ρ	$\sim 10^{3}$	(kg/m^3)
H_w	$\sim 10^{-5}$-10^{-4}	(m)	T_0	298	(K)
L	$\sim 10^{-2}$-10^{-1}	(m)	ζ	$\leq 10^{-2}$	(V)
n	0.1−1.5	(-)	E_x	$\sim 10^{4}$ -10^{5}	(V/m)
m	$\sim 10^{-3}$ -10^{-2}	(Pa·s^n)	ε	$\sim 10^{-10}$	(C/V·m)
C_{pf}	3760	(J/kg·K)	κ	$\sim 10^{6}$ -10^{7}	(m^{-1})
k_f	0.6-0.7	(W/m·K)	σ	$\sim 10^{-4}$ -10^{-2}	(S/m)
k_w	0.15-1.38	(W/m·K)	u_c	$\sim 10^{-4}$ -10^{-3}	(m/s)

Table 1: Material transport properties and geometrical parameters used for estimating dimensionless parameters from the present analysis.

Figure 2 (a, b and c), show the dimensionless velocity distributions for different values of the fluid behavior index, $n(=0.33, 0.5, 0.8, 1, 1.2, 1.5)$, while keeping $\bar{\kappa}=10, 50, 100$, respectively. Dimensionless velocity was obtained using the generalized Smoluchowski velocity u_c for power-law fluids. It can be seen that the irrespective of the value of the fluid behavior index, the velocity near the center of the microchannel approaches the generalized Smoluchowski velocity; so, the velocity profiles becomes more plug-like as the fluid behavior index decreases and also as the electrokinetic parameter increases. For $n=1$, the Newtonian case is recovered. So, it can be seen, that for values of $n<1$ (pseudoplastic liquids) the velocity profile tends to increase in the flow direction upper Newtonian case $n=1$, while the electro-osmotic effect is clearly marked having the larger values of velocity near of the microchannel wall, because this kind of fluids has smaller wall dynamic viscosity (Zhao et al., 2008). For values of $n>1$ (dilatants liquids) the velocity profile tends to decrease in the flow direction below Newtonian case, while the electro-osmotic effect is less in the wall, having the smaller values of velocity near of the microchannel wall, because this kind of fluids has higher wall dynamic viscosity, having a less influence of the external electric field (Zhao, et al., 2008). The influence of the electrokinetic parameter $\bar{\kappa}$ is clear in this figures, for small values of $\bar{\kappa}(=10)$ indicates a big size of the electric double layer with respect to the size of microchannel (tending to overlap of electric double layers) and therefore a low influence for the external electric field near of the microchannel wall, leaving a parabolic pattern in the velocity profiles of the fluid flow. On the other hand, for values of $\bar{\kappa}(\gg 10)$ indicates a small size of the electric double layer respect to the size of microchannel and therefore a high influence for the external electric field near of the microchannel wall; leaving a plug–like pattern in the velocity profiles of the fluid flow.

Figure 3 compares the behavior of the numerical solution for the temperature profile in the fluid region with the asymptotic solution given by Eq. (69). Results are plotted along the dimensionless length of microchannel, for values of Y(=0, 0.5, 1) and n(=0.5). For this set of parameters, a good accordance between both solutions is obtained. Also, it can be appreciated that the temperature changes are more important in the longitudinal direction than in the transversal direction, as established by Eq. (49).

Once validated the numerical solution with the asymptotic solution in the conjugated heat transfer problem, Figure 4-Figure 7 plots the numerical results for the transversal temperature profiles of the fluid and solid regions in the microchannel. Figure 4 shows the spatial development of the Joule heating induced to the fluid and the wall temperature profiles in the microchannel, along the transversal direction in the middle axial position for different values of $n(=0.33, 0.5, 0.8, 1, 1.2, 1.5)$. The temperature distributions in the fluid region exhibit a parabolic-like pattern while the solid wall exhibits a linear behavior (Tang, 2004b). The highest temperature occurs at the microchannel centerline, therefore, it is clear that the heat generated by Joule heating in the fluid is transferred from the central region to the wall by convection and conduction, then is dissipated through the microchannel wall by conduction, and finally is transferred to the surroundings by effect of q_0''. It can be seen that for increasing values of the fluid behavior index the velocity profiles decrease, causing a reduction of convective heat transfer effect and also an increment of the temperature profiles.

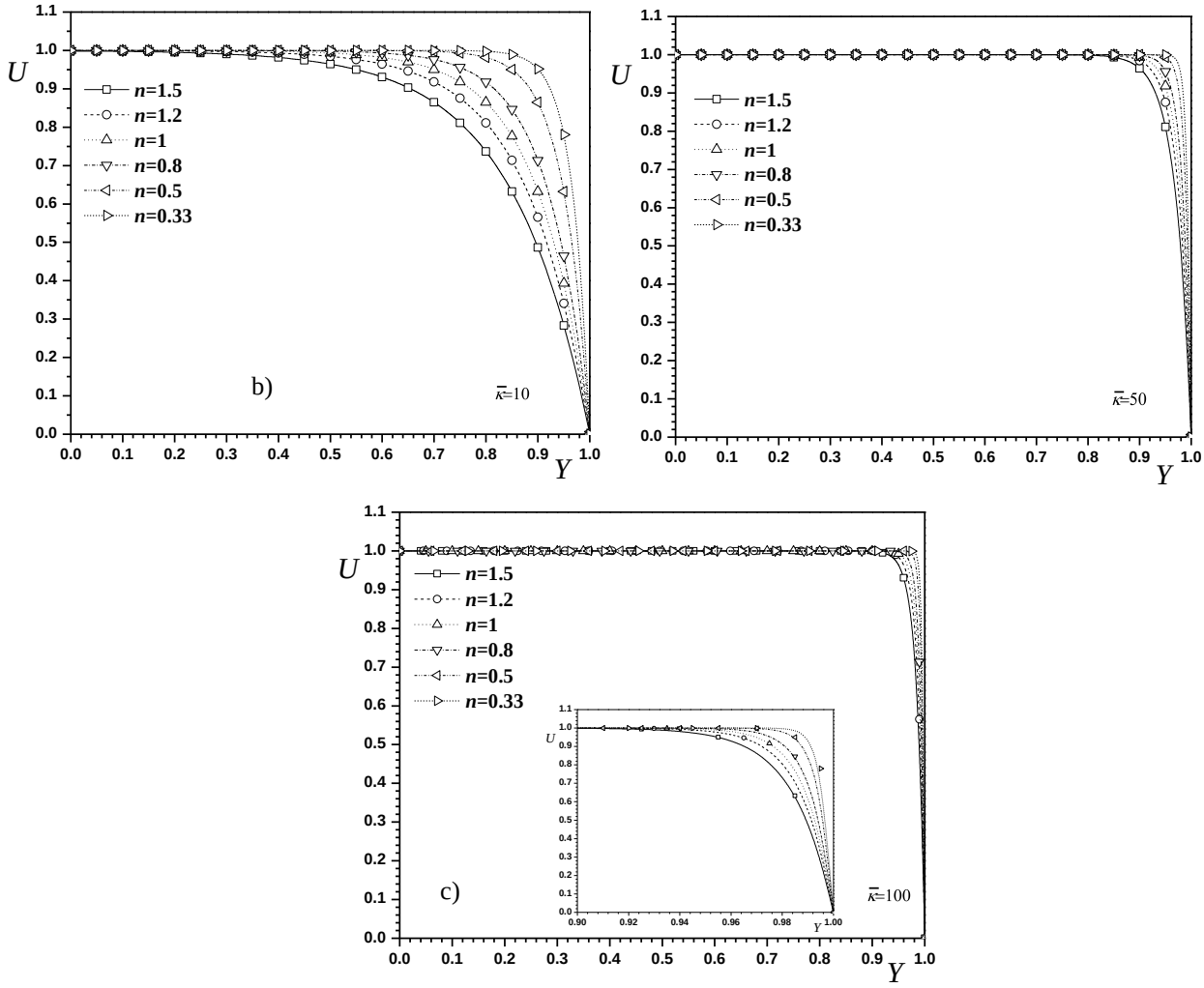

Figure 2: Dimensionless velocity distributions for different values of the fluid behavior index, *n*, while keeping a) $\bar{\kappa}=10$, (adapted Zhao et al., 2008), b) $\bar{\kappa}=50$ and c) $\bar{\kappa}=100$.

Figure 5 shows the evolution of the temperature profiles for different values of Peclet number; when *Pe* decreases, the convection effect decreases also, therefore the temperature increases significantly. So, the *Pe* number is an indicator of the convection velocity in the system. The effect of the fluid behavior index $n>1$ and $n<1$ is the same in Figure 4.

Figure 6 depicts the temperature profiles across transversal direction of microchannel in the middle axial length for the fluid and solid region, for Λ (=1, 0.75, 0.5) and n (=0.5, 1.5). In all cases, the value of q_0'' is considered as a constant extraction of heat from the channel walls. The important temperature changes in electro-osmotic flow, may be attributed to the combined mechanism of Joule heating and heat transfer to the walls. For the cases studied in Figure 6, the Joule heating is the dominant mechanism responsible of temperature increments within the system. In general, as Joule heating increases, the transversal temperature also tends to increases. So, for the different temperature profiles shown in Figure 6 it can be observed that the lower the value of Λ the higher the temperature at a given axial location of the microchannel, (Das and Chakraborty, 2006).

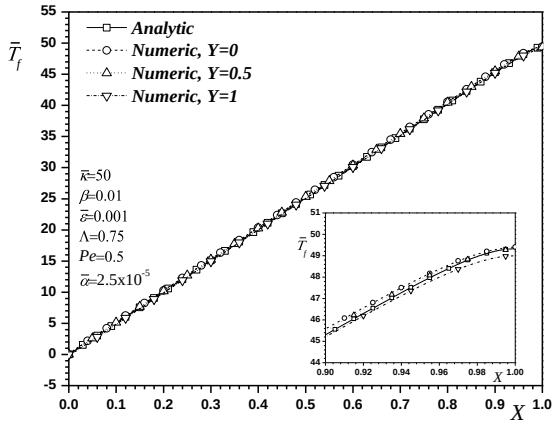

Figure 3: Comparison of the numerical and analytical solution to the temperature profiles in the fluid, along axial direction, for different values of the transversal position, while keeping $n = 0.5$.

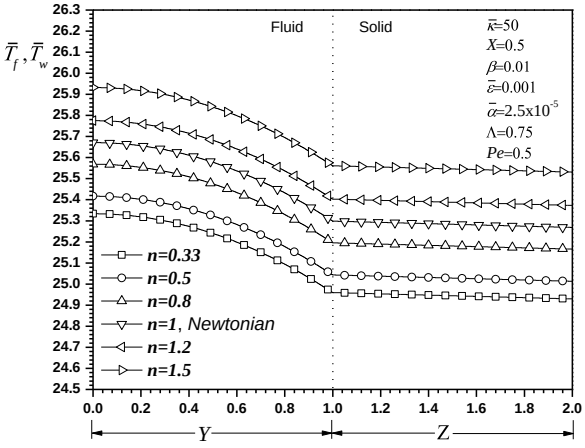

Figure 4: Dimensionless temperature profile as a function of dimensionless transversal coordinate in the fluid and solid region, at X=0.5 for different values of the flow consistency index, n.

Figure 7 shows the dimensionless temperature profiles on a transversal section in the microchannel for different values of $\bar{\alpha}/\bar{\varepsilon}^2 = 25, 2.5, 0.25$, and $n = 0.5, 1.5$. This figure shows that for decreasing values of the parameter $\bar{\alpha}/\bar{\varepsilon}^2$ there is an increase of temperature gradients through the wall of the microchannel; these numerical predictions, are in accordance with the order of magnitude analysis given in section 2.5. For example, $\bar{\alpha}/\bar{\varepsilon}^2 = 25$, corresponds to the limit of the Eq. (57), where prevails $\Delta T_{f,y}/\Delta T_y \sim 1$ and $\Delta T_{w,y}/\Delta T_y \sim \bar{\varepsilon}^2/\bar{\alpha}$. $\bar{\alpha}/\bar{\varepsilon}^2 = 2.5$, corresponds to the limit of the Eq. (56); finally, to $\bar{\alpha}/\bar{\varepsilon}^2 = 0.25$, corresponds to the limit of the Eq. (55). Therefore, for the parameters shown and decreasing values of the $\bar{\alpha}/\bar{\varepsilon}^2$, heat dissipation is slower through the wall of the microchannel, causing significant temperature gradients due to the variation of thermal conductivity and geometry of the wall of the microchannel.

In Figure 8 and Figure 9 the dimensionless entropy generation number for the fluid and solid region is plotted, respectively, as a function of dimensionless longitudinal coordinate for different fluid behavior index $n(= 0.33, 0.5, 0.8, 1, 1.2, 1.5)$. For all cases, the entropy generation decreases toward exit of the microchannel as consequence of the temperature increase in this direction. The entropy generation in the transversal direction is negligible for any value on the index *n*, compared to the entropy generation changes in the longitudinal direction; therefore, inside the fluid or solid regions in the microchannel, the entropy generation rate is of the same order of magnitude for all values of *n*.

Figure 10 shows the influence of the electrokinetic parameter $\bar{\kappa}$ on the dimensionless entropy generation number in the microchannel as a function of the longitudinal coordinate. The entropy generation decreases towards the exit of the microchannel for all values of $\bar{\kappa}$. The main effect of the electrokinetic parameter on the entropy generation is on its transversal distribution. For decreasing values of $\bar{\kappa}$, the entropy generation decreased as a result of the temperature profile and convective heat transfer decrease in the system. For higher values of $\bar{\kappa} > 50$ the N_S changes are negligible. The magnitude of the dimensionless entropy generation number is higher in the fluid region than in the solid one for two reasons. First, the wall thickness is smaller than height of the microchannel, so the fluid region has the largest volume in the microchannel system, and consequently the most important changes in entropy;

and second, because of the significant difference between thermal conductivities of the solid and fluid regions.

In Figure 11, the entropy generation number is presented as a function of the longitudinal coordinate for different values of Peclet number, $Pe(=0.1, 0.25, 0.5, 1, 2.5)$. The entropy generation decreases towards the exit of the microchannel for all values of *Pe*, as temperature increases along the axial coordinate. Being *Pe* a convective heat transfer parameter, when it value tends to increase, the longitudinal temperature drops significantly in the microchannel, leading to an increase of entropy generation in the fluid region. In the case of the microchannel wall, the entropy generation is higher near the *X*=0 position, because it is the zone of lower temperature along the wall of the microchannel and of the whole system.

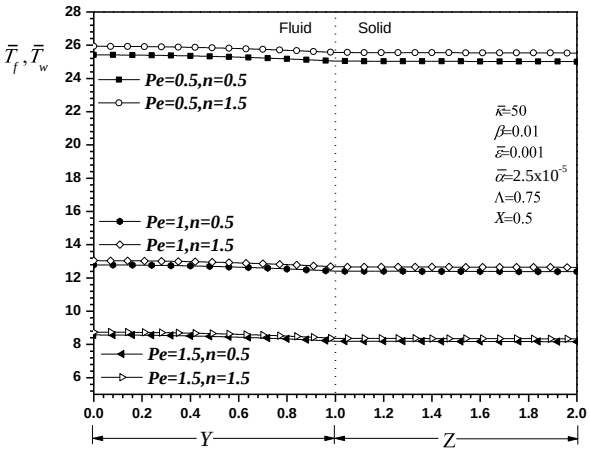

Figure 5: Dimensionless temperature profile as a function of dimensionless transversal coordinate in the fluid and solid region, for different values of the Peclet number, *Pe*, and $n = 0.5, 1.5$.

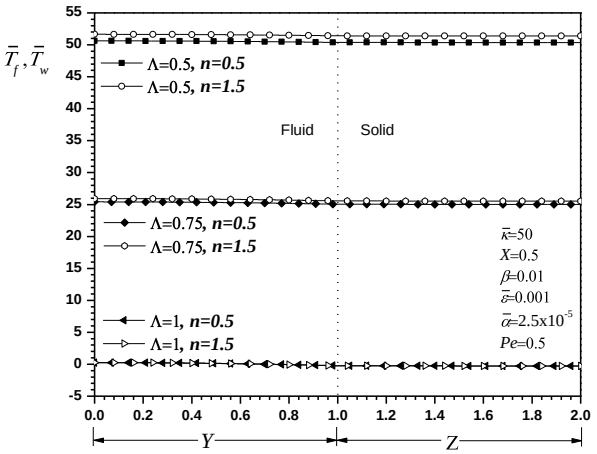

Figure 6: Dimensionless temperature profile as a function of dimensionless transversal coordinate in the fluid and solid region, for different values of the normalized power generation term, Λ, and $n = 0.5, 1.5$.

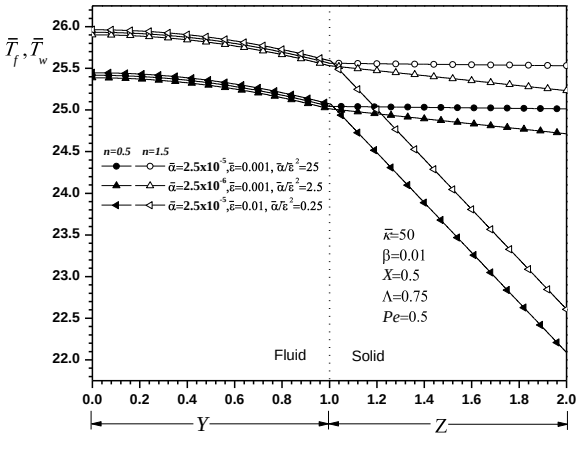

Figure 7: Dimensionless temperature profile as a function of dimensionless transversal coordinate in the fluid and solid region, for different values of parameter, $\bar{\alpha}/\bar{\varepsilon}^2$, and $n = 0.5, 1.5$.

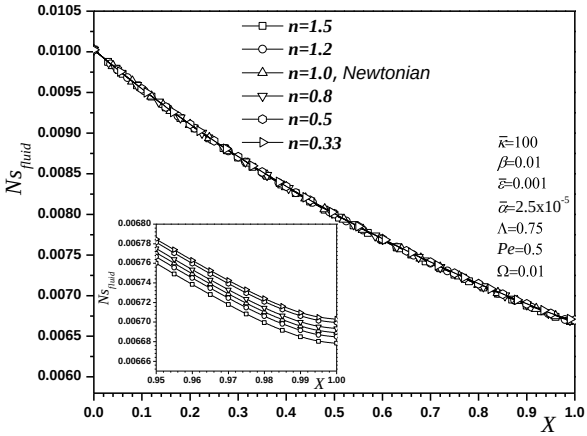

Figure 8: Entropy generation number for the fluid region as a function of dimensionless axial coordinate, for different values of index *n*.

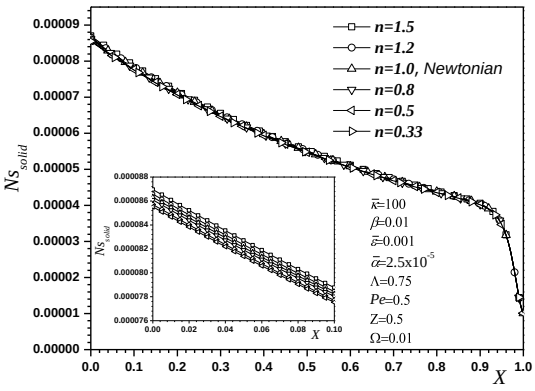

Figure 9: Entropy generation number for the solid region as a function of dimensionless axial coordinate, for different values of index n.

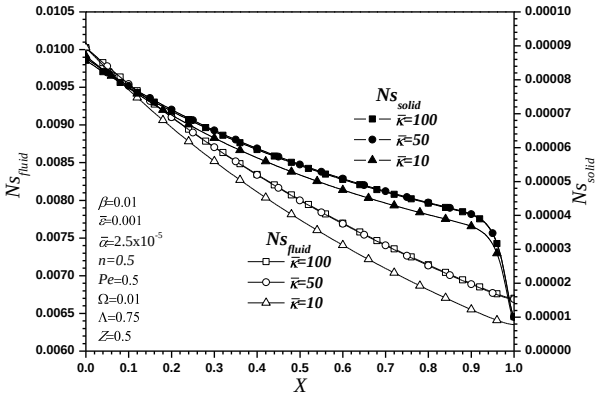

Figure 10: Entropy generation number for the microchannel as a function of dimensionless axial coordinate, for different values of electrokinetic parameter $\bar{\kappa}$.

Figure 12 shows the entropy generation number as a function of the axial coordinate for different values of parameter $\Lambda(=0.5,0.75,1)$. The entropy generation decreases towards exit of the microchannel for any value of Λ, as temperature increases along the axial coordinate. When increasing Λ, the longitudinal microchannel temperature drops significantly, leaving an increase of entropy generation in the fluid region, dictated by Eqs. (78) and (81-82).

In general Figure 13 and Figure 14 show the entropy generation number as a function of the axial coordinate for different values of the parameters, $\bar{\alpha}/\bar{\varepsilon}^2(=25, 2.5, 0.25)$ and $\Omega(=0.01, 0.001, 0.0001)$, respectively. The entropy generation decreases towards the exit of the microchannel for any values of $\bar{\alpha}/\bar{\varepsilon}^2$ and Ω, as temperature increases along the axial coordinate. In Figure 13, the magnitude of entropy generation for any value of $\bar{\alpha}/\bar{\varepsilon}^2$ in the fluid region is the same. In the solid region the effect of the thermal properties of the material and geometry of the microchannel wall is very important. For decreasing values of $\bar{\alpha}/\bar{\varepsilon}^2$ the temperature of the wall of the microchannel decreases significantly increasing the entropy generation. In Figure 14, the magnitude of the entropy generation is strongly linked to the characteristic temperature variation in the system; so, with large changes in temperature (increasing values of parameter Ω), higher values of entropy generation rates are obtained, dictated by Eqs. (78) and (81-83).

In this context, the irreversibility ratio is plotted as a function of axial coordinate in Figure 15 for different values of $Y(=0, 0.5, 1)$. For the group of dimensionless parameters shown, it is observed a negligible contribution by viscous dissipation to the entropy generation in the system. The highest local generation entropy by viscous dissipation is at the microchannel inner interface. Figure 16 shows the Bejan number as a function of axial coordinate, for different values of Peclet number, $Pe(=1, 0.5, 0.25, 0.1)$. For any case, the entropy generation by viscous dissipation is negligible, so that, the second law analysis for this problem is dominated by the heat transfer process. Figure 17 shows the average entropy generation as a function of behavior index n, for different values of $\Lambda(=0.5, 0.75, 1)$. It is clearly seen that the entropy generation is less dependent on flow behavior index, n, but strongly dependent on the power generation parameter, increasing the $\bar{N}_S$ value as Λ increases.

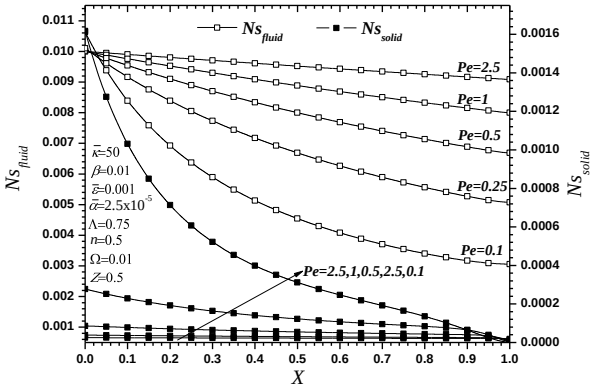

Figure 11: Entropy generation number for the microchannel as a function of dimensionless axial coordinate, for different values of Peclet number, Pe.

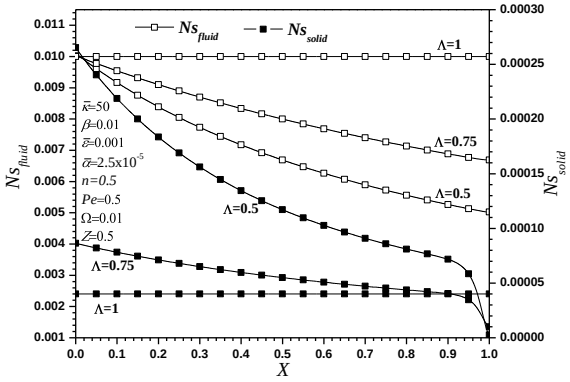

Figure 12: Entropy generation number for the microchannel as a function of dimensionless axial coordinate, for different values of parameter, Λ.

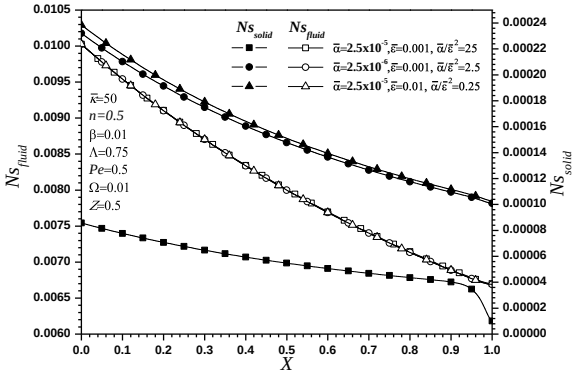

Figure 13: Entropy generation number for the microchannel as a function of dimensionless axial coordinate, for different values of parameter, $\bar{\alpha}/\bar{\varepsilon}^2$.

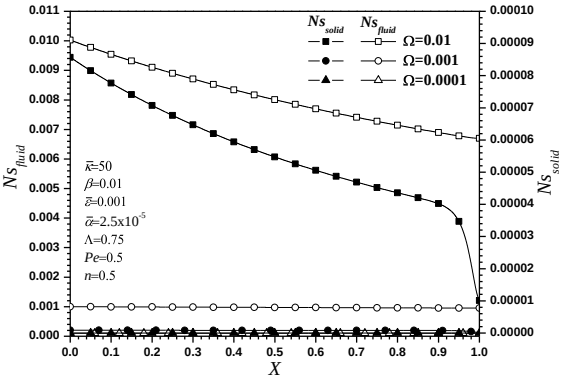

Figure 14: Entropy generation number for the microchannel as a function of dimensionless axial coordinate, for different values of parameter, Ω.

Complementary, Table 2 and Table 3 show the comparison between the numerical and asymptotic solutions for the reduced Nusselt number, evaluated for different longitudinal positions X and for different values of the dimensionless presented parameters. Table 2 shows the independence of the Nusselt number with the dimensionless parameters n, $\bar{\kappa}$, Pe and Λ, as indicated by Eq. (74), and dependence only on the parameter $\bar{\alpha}/\bar{\varepsilon}^2$ (see also Table 3).

4 CONCLUSIONS

For any heat transfer and fluid flow process the entropy generation is associated with thermodynamic irreversibility. The present work we studied the local and global entropy generation of electro-osmotic flow in a parallel flat plate microchannel. The local entropy generation is greater in the region of the fluid than in the wall of microchannel, being higher the entropy generation contribution by Joule heating and negligible by viscous dissipation. In general the entropy generation in this work is dominated by heat transfer process, dictated by the value of Bejan number. There is a strong dependence of the entropy generation rate with the Peclet number, the power generation term, the conjugation term and the characteristic temperature difference; but a weak dependence with any flow behavior index and large values of electrokinetic parameter. The present investigation contributes towards the understanding of the different interconnected transport mechanisms in the design of microfluidic systems.

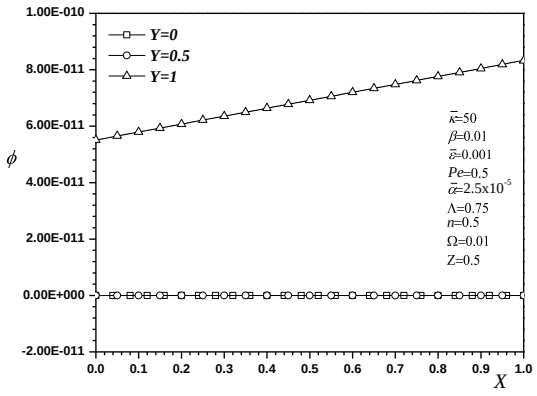

Figure 15: Irreversibility distribution ratio as a function of dimensionless axial coordinate, for different values of transversal coordinate, Y.

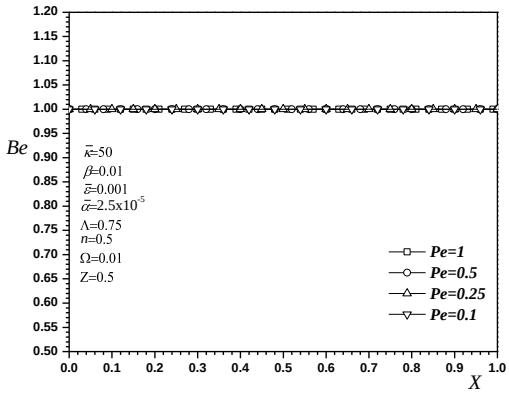

Figure 16: Bejan number as a function of dimensionless axial coordinate, for different values of Peclet number, *Pe.*

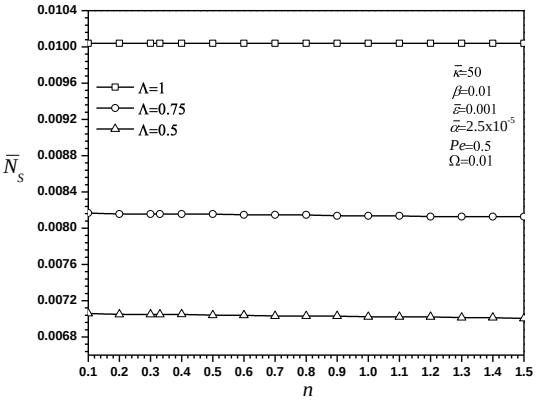

Figure 17: Average entropy generation number as a function of fluid index, for different values of parameter, Λ.

	Nu_N								Nu_A
X	n = 0.5	n = 1.5	$\bar{\kappa}$ = 10	$\bar{\kappa}$ = 100	Pe = 0.5	Pe = 1	Λ = 0.75	Λ = 1.0	
0.1	49.8343	49.8329	49.8343	49.8343	49.8329	49.8342	49.8343	49.8648	50
0.5	49.8387	49.8373	49.8387	49.8387	49.8373	49.8386	49.8387	49.8658	50
1.0	51.2909	51.4564	51.5045	51.2909	51.4564	51.5257	51.2909	49.8683	50

Table 2: Reduced Nusselt number, evaluated at different axial positions and for different values of dimensionless parameters, and $\bar{\alpha}/\bar{\varepsilon}^2 = 25$. The subscript *A* refers to asymptotic solution and subscript *N* denotes numerical solution.

	$\bar{\alpha}$ = 2.5x10^{-5}, $\bar{\alpha}/\bar{\varepsilon}^2$ = 25		$\bar{\alpha}$ = 2.5x10^{-6}, $\bar{\alpha}/\bar{\varepsilon}^2$ = 2.5		$\bar{\alpha}$ = 2.5x10^{-5}, $\bar{\alpha}/\bar{\varepsilon}^2$ = 0.25	
X	Nu_N	Nu_A	Nu_N	Nu_A	Nu_N	Nu_A
0.1	49.8343	50	4.9832	5	0.4983	0.5
0.5	49.8387	50	4.9833	5	0.4983	0.5
1.0	51.2909	50	5.0072	5	0.5128	0.5

Table 3: Reduced Nusselt number, evaluated at different axial positions and for three values of $\bar{\alpha}/\bar{\varepsilon}^2 = 25, 2.5, 0.25$ with $\bar{\kappa} = 50, n = 0.5, Pe = 0.5$ and $\Lambda = 0.75$. The subscript *A* refers to asymptotic solution and subscript *N* denotes numerical solution.

5 ACKNOWLEDGMENTS

This work was supported by a grant 58817 SEP-CONACYT, and 20111013/200110219 SIP-IPN at Mexico.

6 NOMENCLATURE

Be	Bejan number
C_p	specific heat [J/kg·K]
Ec	modified Eckert number
E_x	electric field [V/m]
H	half of microchannel [m]
H_w	wall thickness of the microchannel [m]
k	thermal conductivity [W/m·K]
L	length of microchannel [m]
m	flow consistency index [Pa·s^n]
n	flow behavior index
Nu	Nusselt number
N_S	local entropy generation rate
$\bar{N}_S$	volumetric average entropy generation rate
Pe	Peclet number
Pr	Prandtl number
q_0''	heat flux at the wall in the region $0 \le x \le L$ [W/m^2]
S_G'''	local volumetric entropy [W/m^3·K]
T	temperature [K]
T_0	microchannel inlet temperature [K]
$\bar{T}$	dimensionless temperature
u	fluid axial velocity [m/s]
U	dimensionless fluid axial velocity
u_c	generalized Smoluchowski velocity for power law fluids [m/s]
x	axial coordinate [m]
X	dimensionless axial coordinate
y	transversal coordinate [m]
Y	dimensionless transversal coordinate in the fluid region
Z	dimensionless transversal coordinate in the solid wall

Greek symbols

$\bar{\alpha}$	conjugation term
β	aspect ratio of the fluid region
ΔT_c	characteristic temperature change
ε	dielectric constant [C/V·m]
$\bar{\varepsilon}$	aspect ratio of the solid region
ζ	zeta potential in the shear plane of the electric double layer [V]
κ	inverse Debye length [m^{-1}]
κ^{-1}	Debye length [m]
$\bar{\kappa}$	electrokinetic parameter
Λ	ratio of heat flux from the external wall to the Joule heating
ρ	fluid density [kg/m^3]

ρ_e net charge density [C/m^3]
σ electrical conductivity of the fluid [S/m]
τ_{yx} shear stress [N/m^2]
ϕ irreversibility distribution ratio
Ω dimensionless temperature difference

Subscripts

f fluid
w wall

REFERENCES

Abbassi H., Entropy generation analysis in a uniformly heated microchannel heat sink. *Energy*, 32:1932-1947, 2007.

Bejan A., *Entropy generation minimization*. CRS Press, New York, 1996.

Berli C.L.A., Olivares M.L., Electrokinetic flow of non-Newtonian fluids in microchannels, *Journal of Colloid and Interface Science*, 320: 582–589, 2008.

Das S., Chakraborty S., Analytical solutions for velocity, temperature and concentration distribution in electroosmotic microchannel flows of a non-Newtonian bio-fluid, *Analytica Chimica Acta*, 559: 15–24, 2006.

Hoffman J.D., *Numerical Methods for Engineers and Scientist*. Marcel Dekker, Inc., Chap. 5, 9, 2001.

Ibáñez G., Cuevas S., Entropy generation minimization of a MHD (magnetohydrodynamic) flow in a microchannel. *Energy*, 35:4149-4155, 2010.

Li D., *Electrokinetics in Microfluidics*. Interface Science and Technology, Elsevier Academy Press, V. 2, 2004.

Mahmud S., Fraser R. A., Second law analysis of forced convection in a circular duct for non-Newtonian fluids. *Energy*, 31:2226-2244, 2006.

Masliyah J. H., Bhattacharjee S., *Electrokinetic and Colloid Transport Phenomena*. Wiley Interscience, 2006.

Paolleti S., Rispoli F., Sciubba E., Calculation of exergetic losses in compact heat echanger passages. *ASME AES*, 10:21-9, 1989.

Steffen H., Friedhelm S., Microfluidic Technologies for Miniaturized Analysis Systems. Chapter 2, Springer US, 2007.

Tang G., Yan D., Gong H., Chai C. and Lam Y., Joule heating and its effects on electrokinetic transport of solutes in rectangular microchannels. *Sensors and Actuators A*, 139:221-232, 2007.

Tang G.H., Li X.F., He Y.L., Tao W. Q, Electroosmotic flow of non-Newtonian fluid in microchannels, *Journal of Non-Newtonian Fluid Mechanics*, 157: 133–137, 2009.

Tang G.Y., Yang C., Chai C.K., and Gong H.Q., Numerical analysis of the thermal effect on electroosmotic flow and electrokinetic mass transport in microchannels, *Analytica Chemica Acta*, 507: 27–37, 2004b.

Tang G.Y., Yang C., Chai J.C., Gong H.Q., Joule heating effect on electroosmotic flow and mass species transport in microcapillary. *International Journal of Heat and Mass Transfer*, 47:215–227, 2004a.

Xuan X., Sinton D., Li D., Thermal end effects on electroosmotic flow in a capillary, *International Journal of Heat and Mass Transfer*, 47:3145–3157, 2004a.

Xuan X., Xu B., Sinton D. and Li D., Electroosmotic flow with Joule heating effects. *Miniaturisation for Chemistry, Biology & Bioengineering Lab Chip*, 4:230–236, 2004b.

Zhao C., Zholkovskij E., Masliyah J. H., and Yang C., Analysis of electroosmotic flow of power-law fluids in a slit microchannel. *Journal of Colloid and Interface Science*, 326:503-510, 2008.

Zhao L., Liu L. H., Entropy generation analysis of electro-osmotic flow in open-end and closed-end micro-channels. *International Journal of Thermal Sciences*, 49:418-427, 2010.